Journal of Physics:
Condensed Matter

Ultrafast optical induction of magnetic order at a quantum critical point

To cite this article: Benedikt Fauseweh and Jian-Xin Zhu 2025 *J. Phys.: Condens. Matter* **37** 075603

OPEN ACCESS
IOP Publishing
Journal of Physics: Condensed Matter
J. Phys.: Condens. Matter **37** (2025) 075603 (8pp)
https://doi.org/10.1088/1361-648X/ad9659

Ultrafast optical induction of magnetic order at a quantum critical point

Benedikt Fauseweh[1,2,*] **and Jian-Xin Zhu**[1,3]

[1] Theoretical Division, Los Alamos National Laboratory, Los Alamos, NM 87545, United States of America
[2] Department of Physics, TU Dortmund University, Otto-Hahn-Str 4, 44227 Dortmund, Germany
[3] Center for Integrated Nanotechnologies, Los Alamos National Laboratory, Los Alamos, NM 87545, United States of America

E-mail: benedikt.fauseweh@tu-dortmund.de and jxzhu@lanl.gov

Received 13 September 2024, revised 16 November 2024
Accepted for publication 22 November 2024
Published 6 December 2024

Abstract

Time-resolved ultrafast spectroscopy has emerged as a promising tool to dynamically induce and manipulate non-trivial electronic states of matter out-of-equilibrium. Here we theoretically investigate light pulse driven dynamics in a Kondo lattice system close to quantum criticality. Based on a time-dependent auxiliary fermion mean-field calculation we show that light can dehybridize the local Kondo screening and induce oscillating magnetic order out of a previously paramagnetic state. Depending on the laser pulse field amplitude and frequency the Kondo singlet can be completely deconfined, inducing a dynamic Lifshitz transition that changes the Fermi surface topology. These phenomena can be identified in harmonic generation and time-resolved angle-resolved photoemission spectroscopy spectra. Our results shed new light on non-equilibrium states in heavy fermion systems.

Supplementary material for this article is available online

Keywords: non-equilibrium phase transition, lifshitz transition, high harmonic generation, heavy fermion systems

1. Introduction

Quantum materials exhibit emergent properties that are the result of strong interactions between their constituents, defying a theoretical description in terms of free electrons. Their physical phenomena, such as superconductivity, long range entanglement and topologically protected currents, are exotic and absent in simple metals or insulators [1]. This makes them promising candidates for applications in future quantum devices.

Classifying and predicting such unusual states of matter and their excitation spectra in terms of broken symmetries and topological properties is one of the central aims in modern condensed matter physics. Quantum critical points [2–4] (QCPs), i.e. zero temperature phase transitions separating different ground states driven by quantum fluctuations, are especially interesting in this regard. In heavy fermion systems, such as Ce-, and Yb-based compounds [5–7], localized f electrons act as magnetic moments, that are interacting with conduction band electrons via hybridization. The Ruderman–Kittel–Kasuya–Yosida (RKKY) interaction, which is generated from the Kondo interaction but mediated via the conduction band electrons, is competing with the Kondo interaction and favors magnetic ordering. In the large Kondo interaction J limit, the local singlet formation leads to a Kondo screening effect of the

* Author to whom any correspondence should be addressed.

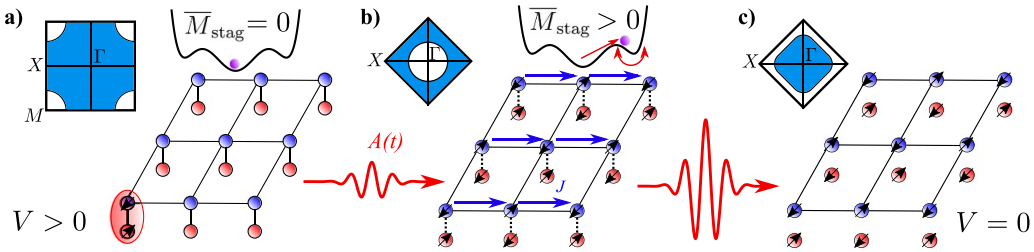

Figure 1. Induction of magnetic order through light-induced dehybridization. (a) Ground state representation of the Kondo lattice model in the Kondo screened PM phase with large FS and no magnetic order. (b) Light-induced staggered magnetization oscillations accompanied with a weakening of the Kondo screening and induced current as indicated by the blue arrows. (c) Further increasing the pulse amplitude completely suppresses the Kondo screening $V=0$.

conduction band electrons. No magnetic order exists and the system is paramagnetic (PM). Due to the strong hybridization between f- and conduction band electrons, the effective mass of the low-energy band electrons gets strongly renormalized and the Fermi surface (FS) volume expands, providing a signature of the Kondo-effect induced heavy Fermi-liquid phase. In contrast if the RKKY interaction dominates, the system exhibits magnetic order and the Kondo heavy quasiparticles are destroyed. The transition between these two phases is nontrivial. In the conventional picture the conduction and f electrons would always hybridize, leading to heavy fermions on both sides of the QCP [8–10]. However, in many experiments a different behavior is observed [5, 11–14], in which a reconstruction of the FS takes place abruptly and the Kondo screening becomes irrelevant. In this case the FS is only determined by the conduction band electrons (small FS). This scenario is referred to as local quantum criticality [7, 15, 16].

While traditional methods to unravel these interesting phenomena in experiment include chemical doping, application of static pressure and magnetic field [17], in recent years it has become possible to use laser pulse femtosecond drives to dynamically induce novel states and non-equilibrium excitations in quantum materials [18–31]. The search for new light induced quantum phases, is a central aim in modern solid state physics [32–34]. A recent highlight is the first experimental discovery of a light-driven Lifshitz transition [35]. Also heavy fermion systems have been investigated in ultrafast experiments [36–39], calling for a theoretical description of the interplay between quantum criticality and non-equilibrium dynamics in these system.

In this work we close this gap by investigating how short laser pulses can influence the local Kondo screening and magnetic order in the Kondo square lattice geometry [40, 41]. Under the assumption of a low frequency pulse, we can safely neglect the local f-interband transitions and purely work with a local magnetic moment degree of freedom. We focus on the uncompensated, metallic regime at $n_c=0.9$, where n_c is the conduction band filling. We use time-dependent mean-field theory supported by time-dependent Variational Monte Carlo (tVMC) calculations to demonstrate, that a dynamical quantum phase transition from a pure Kondo screened PM phase to an oscillating antiferromagnetic state can be induced, see figure 1.

2. Results

The model that we study is the Kondo square lattice model defined by the Hamiltonian

$$H=-t_{\rm hop}\sum_{\langle i,j\rangle,\sigma}\left(c^\dagger_{i\sigma}c_{j\sigma}+\text{H.c.}\right)+J\sum_i \mathbf{S}^c_i\cdot\mathbf{S}^f_i, \tag{1}$$

where the sum $\langle i,j\rangle$ runs over the nearest neighbours. The first term is the kinetic energy of the conduction electrons; the second term is the Kondo coupling of the conduction band to the local $SU(2)$ moments $\mathbf{S}^f_i$ of the f-electrons, with its strength denoted by J. We include a time-dependent EM field by the well established Peierls substitution [42–44]

$$t_{\rm hop}\rightarrow t_{\rm hop}e^{i\mathbf{A}(\tau)(\mathbf{r}_i-\mathbf{r}_j)}, \tag{2}$$

where $\mathbf{A}(t)$ is the time-dependent vector potential.

We use a fermion description of the local magnetic moments $S^\alpha_i=1/2\sum_{\sigma,\sigma'}f^\dagger_{i,\sigma}\tau^\alpha_{\sigma,\sigma'}f_{i,\sigma'}$ leading to the purely fermionic Hamiltonian

$$\begin{aligned}H=&-\sum_{i,j\in\{\mathrm{NN}(i)\},\sigma}t_{\rm hop}e^{i\mathbf{A}(\tau)(\mathbf{r}_i-\mathbf{r}_j)}c^\dagger_{i\sigma}c_{j\sigma}+\text{h.c.}\\&+J/4\sum_{i,\alpha,\{\sigma^{(j)}\}}c^\dagger_{i,\sigma}c_{i,\sigma^{(1)}}f^\dagger_{i,\sigma^{(2)}}f_{i,\sigma^{(3)}}\tau^\alpha_{\sigma,\sigma^{(1)}}\tau^\alpha_{\sigma^{(2)},\sigma^{(3)}},\end{aligned} \tag{3}$$

where $\tau^\alpha_{\sigma,\sigma'}$ are the Pauli matrix components. By constraint, there is on average only one f-electron per site. To proceed further, we consider a decoupling of Kondo exchange interaction using auxiliary fields in the particle-hole channel and introducing *A/B* sublattices for staggered magnetization, leading to self-consistency equations for the quantities

$$2m_{f,A/B}=\left\langle f^\dagger_{i,A/B,\uparrow}f_{i,A/B,\uparrow}\right\rangle-\left\langle f^\dagger_{i,A/B,\downarrow}f_{i,A/B,\downarrow}\right\rangle \tag{4}$$

$$2m_{c,A/B}=\left\langle c^\dagger_{i,A/B,\uparrow}c_{i,A/B,\uparrow}\right\rangle-\left\langle c^\dagger_{i,A/B,\downarrow}c_{i,A/B,\downarrow}\right\rangle \tag{5}$$

$$V_{A/B}=\left\langle c^\dagger_{i,A/B,\uparrow}f_{i,A/B\uparrow}\right\rangle. \tag{6}$$

For convenience we introduce the total and staggered hybridizations

$$V=\frac{1}{2}\left(V_A+V_B\right) \tag{7}$$

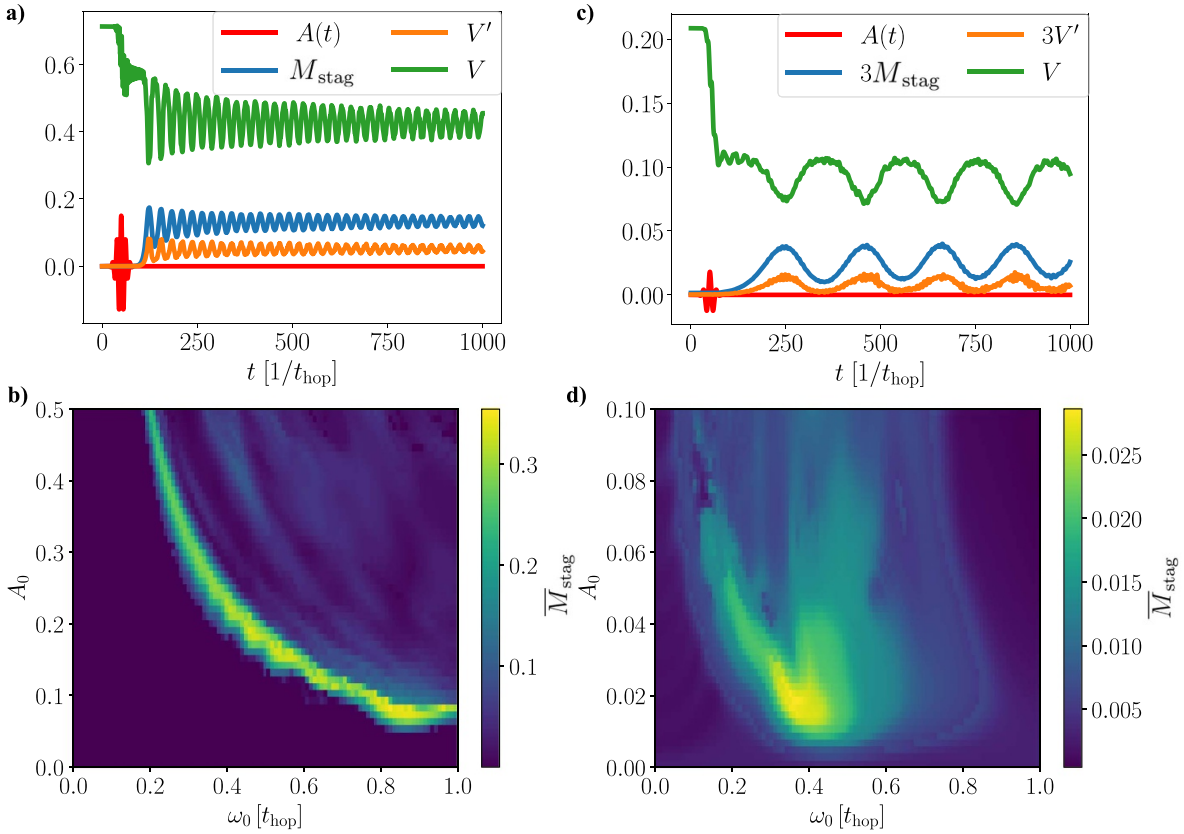

Figure 2. Time-dependence and long-time average of magnetic order parameter and hybridization. (a) Time dependence of staggered magnetization (blue line), total hybridization (green line) and staggered hybridization (orange line) during a short light pulse (red line) in the PM phase at $J = 3.1t_{\mathrm{hop}}$ and $T = 0.01t_{\mathrm{hop}}$. (b) Dynamical phase diagram of the time averaged staggered magnetization M_{stag} after light-pulse as function of pulse amplitude A_0 and frequency ω_0 in the paramagnetic phase at $J = 3.1t_{\mathrm{hop}}$ and effectively zero temperature $T = 0.01t_{\mathrm{hop}}$. (c) Same as in (a) but in the in the intermediate phase with $J = 2.7t_{\mathrm{hop}}$ and $T = 0.195t_{\mathrm{hop}}$ above the Néel temperature. (d) Same as in (b) but in the in the intermediate phase phase with $J = 2.7t_{\mathrm{hop}}$ and $T = 0.195t_{\mathrm{hop}}$ above the Néel temperature.

$$V' = \frac{1}{2}\left(V_A - V_B\right). \tag{8}$$

The introduction of *A/B* sublattices is necessary to allow the breaking of the translational symmetry to accomodate the formation of antiferromagnetic order due to the laser driven temporal fluctuations. This is very similar to the situation in equilibrium.

The auxiliary-field saddle-point approach is capable of qualitatively capturing the ground state phase diagram correctly when compared to more sophisticated methods, such as VMC and dynamical cluster approximation, see [40, 41, 45]. The main difference lies in the energy scale of the phase transitions. VMC shows a transition from the Kondo screened PM phase at large Kondo interaction to an intermediate antiferromagnetic state with hole-like FS at $J = 1.35t_{\mathrm{hop}}$, while the auxiliary-field approach predicts this transition at $J = 3.0t_{\mathrm{hop}}$. The transition to the electron-like FS occurs at $J = 1.1t_{\mathrm{hop}}$ in VMC, while the same transition appears at $J = 2.4t_{\mathrm{hop}}$ in the auxiliary-field approach. Note that the auxiliary-field approach conserves the total number of excitations at fixed momentum k in the reduced Brillouin zone and therefore describes elastic scattering. We caution that inelastic scattering processes will lead to additional damping in the time evolution, which is neglected in our current work. Therefore, we expect that the mean-field approach captures the leading temporal fluctuations and qualitatively describes the non-equilibrium dynamics. A difficulty that emerges in the time-dependent case is the mixing of particle numbers in the c and f sections due to the time-dependence of the hybridization. To fixate the f electron and c electron occupation separately we used time-dependent chemical potentials, see the supplementary note 1 for details.

In equilibrium, three different phases can be distinguished depending on Kondo interaction strength at zero temperature, see supplementary figure 1. We focus on the PM Kondo screened phase at $J = 3.1t_{\mathrm{hop}}$. We parameterize the light pulse using a Gaussian envelope $\mathbf{A}(t) = A_0\mathbf{e}_x \exp(-(t - t_c)^2/2t_d^2)\cos(\omega_0(t - t_c))$, where $t_c = 50/t_{\mathrm{hop}}$ is the pulse center, $t_d = 10/t_{\mathrm{hop}}$ is the pulse width, A_0 is the overall pulse amplitude and ω_0 is the pulse frequency that we are going to vary in the following. We only consider a linear polarization along the x direction. Figure 2(a) shows a typical time evolution of the system as well as the time dependence of the light vector potential. During the laser pulse the Kondo screening diminishes, signaled by the reduction of the total hybridization V between local moments and conduction band electrons. At this

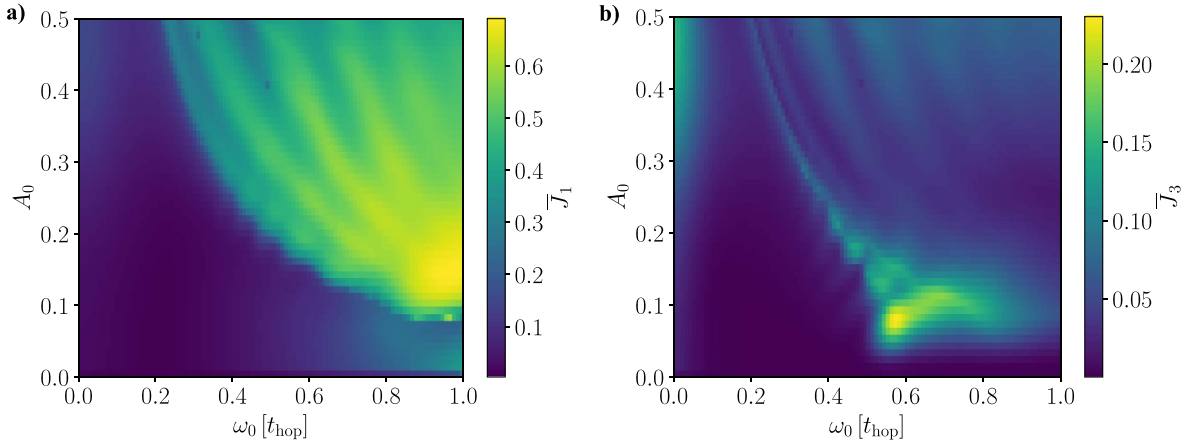

Figure 3. Time averaged induced current. Intensity of the fundamental harmonic (a) and third harmonic (b) after a short light pulse in the PM phase at $J = 3.1t_{\mathrm{hop}}$ and $T = 0.01t_{\mathrm{hop}}$.

point in time the RKKY interaction induces the formation of long range magnetic order M_{stag} directly after the pulse. This qualitative behavior, i.e. an enhancement of magnetic correlations by the light pulse, is supported by tVMC calculations in the supplementary note 2. The structure of this magnetic order is identical to the intermediate equilibrium regime but the order parameter oscillates around its asymptotic value $\overline{M}_{\mathrm{stag}}$. These order parameter oscillations are similar to the recently observed Higgs oscillations in superconducting condensates. Similar to the Higgs oscillations, the oscillation frequency is proportional to the asymptotic order parameter value. At the same time we observe hybridization oscillations with the same frequency but with a π-phase shift. A finite staggered component V' dynamically evolves after the pulse, which is in phase with respect to the antiferromagnetic order parameter oscillations. We observe only a very slow decay of the oscillations, indicating the formation of a stable collective magnetic excitation. Note that the simulations by tVMC does not show oscillations of the spin correlations. We attribute this fact to the limited system size accessible in these simulations, which introduce spurious boundary effects. To quantify the dependence of the induced staggered magnetization on the pulse parameters, we investigate the dynamical phase diagram (DPD) of the asymptotic staggered magnetization in figure 2(b) as function of pulse amplitude and frequency. In order to induce a finite staggered magnetization, pulse frequency ω_0 and amplitude A_0 have to be sufficiently large. Once a certain threshold value is reached we observe a dispersive region in which the induced staggered magnetization is maximized. Further enhancing the pulse amplitude does not result in an increased staggered magnetization but instead heats the system, melting the induced staggered magnetization again. Within this region, we can still induce magnetic order parameter oscillations, however their asymptotic value is close to zero. The possibility to dynamically induce magnetic order out of an unordered state is not limited to the zero temperature case. In figure 2(c) we investigate the system dynamics within the intermediate regime, i.e. $J = 2.7t_{\mathrm{hop}}$ and $T = 0.195t_{\mathrm{hop}}$, which is above the Néel temperature, $T_{\mathrm{N}} \approx 0.185t_{\mathrm{hop}}$, but still within the Kondo screened phase. After the initial hybridization drop, we observe the dynamical formation of magnetic order. The overall amplitude of the induced staggered magnetization is reduced when compared to the zero temperature case, resulting in slower order parameter oscillations. The corresponding finite temperature DPD of the asymptotic staggered magnetization is shown in figure 2(d). It shows a much broader region of induced staggered magnetization, compared to the zero temperature case.

To identify the dynamical phase transition in experiment we investigate the high harmonic generation (HHG) [46] spectrum induced by the pump pulse. Specifically we concentrate on the intensity profiles of the fundamental and third harmonic as a function of pulse amplitude and frequency for the zero temperature case. As shown in figure 3 the fundamental harmonic shows a strong response upon entering the Kondo breakdown regime, see for comparison figure 2(b). The third harmonic is also sensitive to the magnetic phase transition. Additionally it features a strong response for $A_0 \approx 0.07t_{\mathrm{hop}}$ and $\omega_0 \approx 0.58t_{\mathrm{hop}}$, just before the actual breakdown of the Kondo screening at stronger pump pulses. The strong sensitivity of the HHG spectra to the phase transition can be understood in terms of a breakdown of the Kondo screening, leading to a creation of free charge carriers.

Using only HHG spectroscopy we can pinpoint the transition region but it is insufficient to directly investigate the microscopic non-equilibrium dynamics. We thus use the method introduced by Freericks, Krishnamurthy and Pruschke [47] to compute time-resolved angle-resolved photoemission spectroscopy (tr-ARPES) spectra. To resolve the light pulse induced dynamics directly, we need a pulse that is short enough to not average over the dynamics, while being long enough to obtain a sufficient energy resolution. Figures 4(a)–(c) shows the order paramter oscillations, including the probe pulse as shaded regions, the ARPES signal centered around t_1 and t_2, respectively. The magnetic order oscillations directly manifest in oscillation of the spectral function in energy and

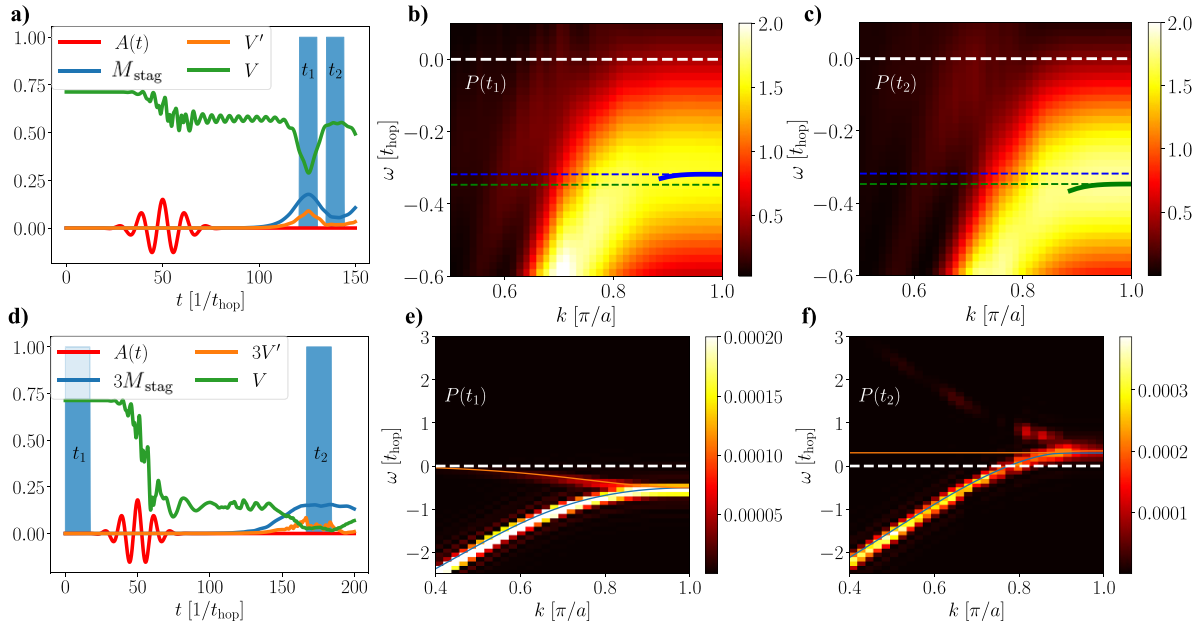

Figure 4. Order parameter oscillations and Lifshitz transition in time-resolved ARPES. (a) Dynamics after pump pulse inducing order parameter oscillations for $A_0 = 0.15$ and $\omega_0 = 0.55/t_{\mathrm{hop}}$. Shaded regions show the time domain for the photoemission spectroscopy probe pulses. (b) and (c) Photoemission spectra measured at t_1 and t_2 respectively, as shown in (a). Solid lines show the maximum of the signal as function of k while dotted lines are for comparison. (d) Dynamics for stronger pump pulse that significantly reduces the hybridization. Pulse parameters are $A_0 = 0.18$ and $\omega_0 = 0.55/t_{\mathrm{hop}}$. (e) Photoemission spectra measured at t_1 before the pump pulse as shown in (d). Solid lines are the time averaged lowest eigenvalues of the mean-field Hamiltonian. (f) Photoemission spectra measured at hybridization minimum at t_2 after the pump pulse in (d). Solid lines as in (e). All momenta measured in $k = |(k_x, k_y)|$ for a path along the diagonal in the reduced BZ.

amplitude, see blue (in panel (b)) and green (in panel (c)) lines. Amplitude and energy oscillations have also been proposed to observe superconducting Higgs modes in tr-ARPES type experiments [48–51].

To further elucidate the effect of stronger pump pulses we investigate a case, in which the Kondo screening is more strongly affected. Figures 4(d)–(f) shows the dynamics in which the hybridization is suppressed by up to 90% at t_2, the ARPES signal in equilibrium at t_1 and after the pulse at t_2 respectively. In equilibrium the FS is large within the reduced BZ. After optical excitation the situation changes drastically. The local magnetic moments dehybridize from the conduction band, strongly renormalizing the electronic structure. The FS is now significantly reduced (small FS) and we see excitations in the upper, previously empty, conduction bands. This change in the FS is similar to what is observed in equilibrium when the Kondo destruction induces a topological Lifshitz transition. While the equilibrium transition is triggered by the change of the Kondo interaction strength, here it is driven by fluctuations induced through the strong laser light.

3. Discussion

In conclusion, we have predicted a rare light-induced symmetry breaking in heavy fermion systems accompanied with the destruction of the Kondo coherence. We have shown, that two different types of phase transitions, a second order transition with the appearance of magnetic order and a topological FS reconstruction, can be dynamically driven using ultra-short laser pulses. The laser-induced regime is highly sensitive to the laser pulse parameters and HHG can be used to dynamically map out the phase transition region. Theoretical calculations of tr-ARPES spectra have evidenced the magnetic order parameter oscillations, as well as the Lifshitz transition. It is expected that such a phase transition has a significant effect on transport properties, such as the transient Hall coefficient, which should show a sign change after the topological transition. Our results suggest that the character of the Kondo PM phase is disturbed by the light field, while the formation of magnetic order via the RKKY interaction requires stronger light fields in order to be suppressed. Note that this selectivity is contrary to the effect of pure heating, where temperature fluctuations induce a Néel temperature that is smaller than the Kondo temperature, see supplementary note 1. The dynamically induced properties clearly show that the interplay between light, Kondo effect and magnetic order can have profound effects for heavy fermion materials.

4. Methods

4.1. Time evolution with fixed particle number

During the excitation with the laser pulse, the single occupancy requirement of the f-electrons could be violated, due to hybridization with the conduction band electrons. While this issue is fixed using the chemical potential of the f electrons in equilibrium, in non-equilibrium the problem is more subtle,

as the effect of the chemical potential on the f filling shows up only in second order. In order to avoid an unphysical time evolution we derive a method in order to fix the first derivative of the f electron number with respect to time and thereby also the electron number itself.

We introduce a Nambu spinor representation in the form

$$\mathbf{C}^{\dagger}_{\mathbf{k}\sigma} = \left(c^{\dagger}_{\mathbf{k}\sigma A} c^{\dagger}_{\mathbf{k}\sigma B} f^{\dagger}_{\mathbf{k}\sigma A} f^{\dagger}_{\mathbf{k}\sigma B} \right). \tag{9}$$

Such that the Hamiltonian can be written as

$$H = \sum_{\mathbf{k},\sigma} \mathbf{C}^{\dagger}_{\mathbf{k}\sigma} \underbrace{\begin{pmatrix} \mu_c + J/2\sigma m_f & \epsilon(\mathbf{k}-\mathbf{A}) & -\frac{J}{4}(3V-\sigma V') & 0 \\ \epsilon(\mathbf{k}-\mathbf{A}) & \mu_c - J/2\sigma m_f & 0 & -\frac{J}{4}(3V+\sigma V') \\ -\frac{J}{4}(3V-\sigma V') & 0 & \mu_f + \frac{J}{2}\sigma m_c & 0 \\ 0 & -\frac{J}{4}(3V+\sigma V') & 0 & \mu_f - \frac{J}{2}\sigma m_c \end{pmatrix}}_{\mathbf{H}_{k\sigma}} \mathbf{C}_{\mathbf{k}\sigma}. \tag{10}$$

We go into the Heisenberg picture to describe the time evolution of the Nambu spinor

$$\mathbf{C}_{\mathbf{k}\sigma}(t) = \mathbf{V}_{\mathbf{k}\sigma}(t)\,\mathbf{C}_{\mathbf{k}\sigma} \tag{11}$$

where $\mathbf{V}_{\mathbf{k}\sigma}(t)$ encodes the time evolution in the original operator basis $\mathbf{C}_{\mathbf{k}\sigma}$ The time evolution of an arbitrary bilinear observable O with matrix representation $\mathbf{O}$ can be written as

$$O(t) = \frac{1}{N}\sum_{\mathbf{k},\sigma} \left\langle \mathbf{D}^{\dagger}_{\mathbf{k}\sigma}\mathbf{U}^{\dagger}_{\mathbf{k}\sigma}\mathbf{V}^{\dagger}_{\mathbf{k}\sigma}(t)\,\mathbf{O}\mathbf{V}_{\mathbf{k}\sigma}(t)\,\mathbf{U}_{\mathbf{k}\sigma}\mathbf{D}_{\mathbf{k}\sigma} \right\rangle \tag{12}$$

with

$$i\partial_t \mathbf{V}_{\mathbf{k}\sigma}(t) = \mathbf{H}_{\mathbf{k}\sigma}\mathbf{V}_{\mathbf{k}\sigma}(t). \tag{13}$$

Being the Heisenberg time evolution and $\mathbf{U}_{\mathbf{k}}\mathbf{D}_{\mathbf{k}\sigma} = \mathbf{C}_{\mathbf{k}\sigma}$ being the transformation to the diagonal operator basis. The derivative of an Observable that does not explicitly depend on time reads

$$i\partial_t O(t) = \frac{1}{N}\sum_{\mathbf{k},\sigma} \left\langle \mathbf{D}^{\dagger}_{\mathbf{k}\sigma}\mathbf{U}^{\dagger}_{\mathbf{k}\sigma}\mathbf{V}^{\dagger}_{\mathbf{k}\sigma}(t)\,[\mathbf{O},\mathbf{H}_{\mathbf{k}\sigma}]\,\mathbf{V}_{\mathbf{k}\sigma}(t)\,\mathbf{U}_{\mathbf{k}\sigma}\mathbf{D}_{\mathbf{k}\sigma} \right\rangle. \tag{14}$$

We want to fix the f-electron filling factor during the time evolution by adjusting μ_f in time

$$i\partial_t n_f = \frac{1}{N}\sum_{\mathbf{k},\sigma} \left\langle \mathbf{D}^{\dagger}_{\mathbf{k}\sigma}\mathbf{U}^{\dagger}_{\mathbf{k}\sigma}\mathbf{V}^{\dagger}_{\mathbf{k}\sigma}(t)\,[\mathbf{N}_f,\mathbf{H}_{\mathbf{k}\sigma}]\,\mathbf{V}_{\mathbf{k}\sigma}(t)\,\mathbf{U}_{\mathbf{k}\sigma}\mathbf{D}_{\mathbf{k}\sigma} \right\rangle \tag{15}$$

where

$$\mathbf{N}_f = \begin{pmatrix} 0,0,0,0 \\ 0,0,0,0 \\ 0,0,1,0 \\ 0,0,0,1 \end{pmatrix} \tag{16}$$

is the matrix representation of n_f. This first derivative does not depend on μ_f explicitly, hence we have to go one step further and calculate the second derivative. We first define

$$\begin{aligned} \mathbf{K}_{NH}(t) &= [\mathbf{N}_f, \mathbf{H}_{\mathbf{k}\sigma}] \\ &= \begin{pmatrix} 0 & 0 & J/4(3V-\sigma V') & 0 \\ 0 & 0 & 0 & J/4(3V+\sigma V') \\ -J/4(3V-\sigma V') & 0 & 0 & 0 \\ 0 & -J/4(3V+\sigma V') & 0 & 0 \end{pmatrix}. \end{aligned} \tag{17}$$

Its derivative reads

$$\partial_t \mathbf{K}_{NH}(t) = \begin{pmatrix} 0 & 0 & \frac{J}{4}(3\partial_t V - \sigma\partial_t V') & 0 \\ 0 & 0 & 0 & \frac{J}{4}(3\partial_t V + \sigma\partial_t V') \\ \frac{-J}{4}(3\partial_t V - \sigma\partial_t V') & 0 & 0 & 0 \\ 0 & \frac{-J}{4}(3\partial_t V + \sigma\partial_t V') & 0 & 0 \end{pmatrix}. \tag{18}$$

It depends on the derivatives of the hybridization on the *A/B* sublattice, which read

$$i\partial_t V_{A/B} = i\partial_t \frac{1}{2N}\sum_i \left\langle c^\dagger_{i,A/B,\uparrow} f_{i,A/B\uparrow}\right\rangle + \left\langle f^\dagger_{i,A/B,\uparrow} c_{i,A/B\uparrow}\right\rangle \tag{19}$$

$$= \frac{1}{N}\sum_{\mathbf{k},\sigma}\left\langle \mathbf{D}^\dagger_{\mathbf{k}\sigma}\mathbf{U}^\dagger_{\mathbf{k}\sigma}\mathbf{V}^\dagger_{\mathbf{k}\sigma}(t)\left[\mathbf{V}_{A/B},\mathbf{H}_{\mathbf{k}\sigma}\right]\mathbf{V}_{\mathbf{k}\sigma}(t)\mathbf{U}_{\mathbf{k}\sigma}\mathbf{D}_{\mathbf{k}\sigma}\right\rangle. \tag{20}$$

Now we can calculate the second derivative of the f electron filling factor

$$-\partial_t^2 n_f = \frac{1}{N}\sum_{\mathbf{k},\sigma}\left\langle \mathbf{D}^\dagger_{\mathbf{k}\sigma}\mathbf{U}^\dagger_{\mathbf{k}\sigma}\mathbf{V}^\dagger_{\mathbf{k}\sigma}(t)\left[\mathbf{K}_{NH}(t),\mathbf{H}_{\mathbf{k}\sigma}\right]\mathbf{V}_{\mathbf{k}\sigma}(t)\mathbf{U}_{\mathbf{k}\sigma}\mathbf{D}_{\mathbf{k}\sigma}\right\rangle \tag{21}$$

$$+\left\langle \mathbf{D}^\dagger_{\mathbf{k}\sigma}\mathbf{U}^\dagger_{\mathbf{k}\sigma}\mathbf{V}^\dagger_{\mathbf{k}\sigma}(t)\left(i\partial_t\mathbf{K}_{NH}(t)\right)\mathbf{V}_{\mathbf{k}\sigma}(t)\mathbf{U}_{\mathbf{k}\sigma}\mathbf{D}_{\mathbf{k}\sigma}\right\rangle. \tag{22}$$

We now determine μ_f in a self-consistent loop at each time step, such that the second derivative of n_f vanishes. As long as the external perturbation does not change n_f in a non-continuous way, this also fixes $n_f = 1$.

4.2. tr-ARPES calculation

We compute the PES signal $P(t,\omega,k) = \int\tau_1\int\tau_2 s_t(\tau_1)s_t(\tau_2)\,\mathrm{e}^{\mathrm{i}\omega(\tau_1-\tau_2)}G^<(k,\tau_1,\tau_2)$, where $s_t(\tau)$ is the probe pulse shape function centered around t and $G^<$ is the two-time lesser Green function. Figure 2(a) of the main text shows the probe pulse as shaded regions, parameterized as

$$s_t(\tau) = \begin{cases} 1 & \text{if } t - t_\mathrm{w}/2 < \tau < t + t_\mathrm{w}/2 \\ \mathrm{e}^{-(\tau-(t-t_\mathrm{w}/2))^2/2t_\mathrm{s}^2} & \text{if } \tau \leqslant t - t_\mathrm{w}/2 \\ \mathrm{e}^{-(\tau-(t+t_\mathrm{w}/2))^2/2t_\mathrm{s}^2} & \text{if } \tau \geqslant t + t_\mathrm{w}/2 \end{cases} \tag{23}$$

where t_w is the width of the probe pulse, and t_s is the switching time. We choose $t_\mathrm{s} = 1/t_\mathrm{hop}$ in all calculations while the width is variable. Note that the lesser Green function can be easily calculated within the mean-field description.

Data availability statement

All data that support the findings of this study are included within the article (and any supplementary files).

Acknowledgments

We thank Rohit Prasankumar, Filip Ronning and Qimiao Si for helpful discussions. This work was supported by the U.S. DOE NNSA under Contract No. 89233218CNA000001 via the LANL LDRD Program. It was supported in part by the Center for Integrated Nanotechnologies, a U.S. DOE Office of Basic Energy Sciences user facility, in partnership with the LANL Institutional Computing Program for computational resources.

ORCID iDs

Benedikt Fauseweh https://orcid.org/0000-0002-4861-7101
Jian-Xin Zhu https://orcid.org/0000-0001-7991-3918

References

[1] Keimer B and Moore J E 2017 The physics of quantum materials *Nat. Phys.* **13** 1045–55
[2] Sachdev S 1999 *Quantum Phase Transitions* (Cambridge University Press)
[3] Coleman P and Schofield A J 2005 Quantum criticality *Nature* **433** 226–9
[4] Si Q and Steglich F 2010 Heavy fermions and quantum phase transitions *Science* **329** 1161–6
[5] Stewart G R 2001 Non-fermi-liquid behavior in *d*- and *f*-electron metals *Rev. Mod. Phys.* **73** 797–855
[6] Löhneysen H V, Rosch A, Vojta M and Wölfle P 2007 Fermi-liquid instabilities at magnetic quantum phase transitions *Rev. Mod. Phys.* **79** 1015–75
[7] Gegenwart P, Si Q and Steglich F 2008 Quantum criticality in heavy-fermion metals *Nat. Phys.* **4** 186–97
[8] Hertz J A 1976 Quantum critical phenomena *Phys. Rev.* B **14** 1165–84
[9] Millis A J 1993 Effect of a nonzero temperature on quantum critical points in itinerant fermion systems *Phys. Rev.* B **48** 7183–96
[10] Moriya Tôru and Takimoto T 1995 Anomalous properties around magnetic instability in heavy electron systems *J. Phys. Soc. Japan* **64** 960–9
[11] Coleman P, Pépin C, Si Q and Ramazashvili R 2001 How do fermi liquids get heavy and die? *J. Phys.: Condens. Matter* **13** R723–38
[12] von Löhneysen H 1996 Non-fermi-liquid behaviour in the heavy-fermion system *J. Phys.: Condens. Matter* **8** 9689–706
[13] Schröder A, Aeppli G, Coldea R, Adams M, Stockert O, v. Löhneysen H, Bucher E, Ramazashvili R and Coleman P 2000 Onset of antiferromagnetism in heavy-fermion metals *Nature* **407** 351–5
[14] Güttler M *et al* 2019 Divalent $EuRh_2Si_2$ as a reference for the luttinger theorem and antiferromagnetism in trivalent heavy-fermion $YbRh_2Si_2$ *Nat. Commun.* **10** 796
[15] Si Q, Rabello S, Ingersent K and Lleweilun Smith J 2001 Locally critical quantum phase transitions in strongly correlated metals *Nature* **413** 804–8
[16] Kirchner S, Paschen S, Chen Q, Wirth S, Feng D, Thompson J D and Si Q 2020 Colloquium: Heavy-electron quantum criticality and single-particle spectroscopy *Rev. Mod. Phys.* **92** 011002
[17] Wirth S and Steglich F 2016 Exploring heavy fermions from macroscopic to microscopic length scales *Nat. Rev. Mater.* **1** 16051
[18] Basov D N, Averitt R D and Hsieh D 2017 Towards properties on demand in quantum materials *Nat. Mater.* **16** 1077–88
[19] Fausti D, Tobey R I, Dean N, Kaiser S, Dienst A, Hoffmann M C, Pyon S, Takayama T, Takagi H and Cavalleri A 2011 Light-induced superconductivity in a stripe-ordered cuprate *Science* **331** 189–91
[20] Mankowsky R, Subedi A, Först M, Mariager S O, Chollet M, Lemke H T, Robinson J S, Glownia J M, Minitti M P, Frano A, Fechner M, Spaldin N A, Loew T, Keimer B, Georges A and Cavalleri A 2014 Nonlinear lattice dynamics as a basis for enhanced superconductivity in $YBa_2Cu_3O^{6.5}$

[21] Mitrano M *et al* 2016 Possible light-induced superconductivity in K3C60 at high temperature *Nature* **530** 461–4
[22] Paeckel S, Fauseweh B, Osterkorn A, Köhler T, Manske D and Manmana S R 2020 Detecting superconductivity out of equilibrium *Phys. Rev.* B **101** 180507
[23] Buzzi M *et al* 2020 Photomolecular high-temperature superconductivity *Phys. Rev.* X **10** 031028
[24] Sie E J *et al* 2019 An ultrafast symmetry switch in a weyl semimetal *Nature* **565** 61–66
[25] Seyler K L *et al* 2018 Ligand-field helical luminescence in a 2D ferromagnetic insulator *Nat. Phys.* **14** 277–81
[26] Sun Z *et al* 2019 Giant nonreciprocal second-harmonic generation from antiferromagnetic bilayer Cri_3 *Nature* **572** 497–501
[27] Padmanabhan P *et al* 2022 Coherent helicity-dependent spin-phonon oscillations in the ferromagnetic van der waals crystal cri3 *Nat. Commun.* **13** 4473
[28] Matsunaga R, Hamada Y I, Makise K, Uzawa Y, Terai H, Wang Z and Shimano R 2013 Higgs amplitude mode in the BCS superconductors $Nb_{1-x}Ti_x$**N** induced by terahertz pulse excitation *Phys. Rev. Lett.* **111** 057002
[29] Matsunaga R, Tsuji N, Fujita H, Sugioka A, Makise K, Uzawa Y, Terai H, Wang Z, Aoki H and Shimano R 2014 Light-induced collective pseudospin precession resonating with higgs mode in a superconductor *Science* **345** 1145–9
[30] Schwarz L *et al* 2020 Classification and characterization of nonequilibrium Higgs modes in unconventional superconductors *Nat. Commun.* **11** 287
[31] Chu H *et al* 2020 Phase-resolved higgs response in superconducting cuprates *Nat. Commun.* **11** 1793
[32] Kennes D M, Wilner E Y, Reichman D R and Millis A J 2017 Transient superconductivity from electronic squeezing of optically pumped phonons *Nat. Phys.* **13** 479–83
[33] Yang X *et al* 2018 Terahertz-light quantum tuning of a metastable emergent phase hidden by superconductivity *Nat. Mater.* **17** 586–91
[34] Giorgianni F, Cea T, Vicario C, Hauri C P, Withanage W K, Xi X and Benfatto L 2019 Leggett mode controlled by light pulses *Nat. Phys.* **15** 341–6
[35] Beaulieu S *et al* 2021 Ultrafast dynamical lifshitz transition *Sci. Adv.* **7** eabd9275
[36] Wetli C, Pal S, Kroha J, Kliemt K, Krellner C, Stockert O v, Löhneysen H and Fiebig M 2018 Time-resolved collapse and revival of the Kondo state near a quantum phase transition *Nat. Phys.* **14** 1103–7
[37] Talbayev D *et al* 2010 Hybridization and superconducting gaps in the heavy-fermion superconductor $PuCoGa_5$ probed via the dynamics of photoinduced quasiparticles *Phys. Rev. Lett.* **104** 227002
[38] Leuenberger D, Sobota J A, Yang S-L, Pfau H, Kim D-J, Mo S-K, Fisk Z, Kirchmann P S and Shen Z-X 2018 Dehybridization of f and d states in the heavy-fermion system $YbRh_2Si_2$ *Phys. Rev.* B **97** 165108
[39] Pal S, Wetli C, Zamani F, Stockert O, Löhneysen H v, Fiebig M and Kroha J 2019 Fermi volume evolution and crystal-field excitations in heavy-fermion compounds probed by time-domain terahertz spectroscopy *Phys. Rev. Lett.* **122** 096401
[40] Zhian Asadzadeh M, Becca F and Fabrizio M 2013 Variational monte carlo approach to the two-dimensional kondo lattice model *Phys. Rev.* B **87** 205144
[41] Watanabe H and Ogata M 2007 Fermi-surface reconstruction without breakdown of kondo screening at the quantum critical point *Phys. Rev. Lett.* **99** 136401
[42] Claassen M, Jiang H-C, Moritz B and Devereaux T P 2017 Dynamical time-reversal symmetry breaking and photo-induced chiral spin liquids in frustrated Mott insulators *Nat. Commun.* **8** 1192
[43] Konstantinova T *et al* 2018 Nonequilibrium electron and lattice dynamics of strongly correlated $Bi_2Sr_2CaCu_2O_{8+\delta}$ single crystals *Sci. Adv.* **4** eaap7427
[44] Shen W, Y G, Krishnamurthy H R, Devereaux T P and Freericks J K 2014 Nonequilibrium 'Melting' of a charge density wave insulator via an ultrafast laser pulse *Phys. Rev. Lett.* **112** 176404
[45] Martin L C, Bercx M and Assaad F F 2010 Fermi surface topology of the two-dimensional kondo lattice model: dynamical cluster approximation approach *Phys. Rev.* B **82** 245105
[46] Fauseweh B and Zhu J-X 2020 Laser pulse driven control of charge and spin order in the two-dimensional kondo lattice *Phys. Rev.* B **102** 165128
[47] Freericks J K, Krishnamurthy H R and Pruschke T h 2009 Theoretical description of time-resolved photoemission spectroscopy: application to pump-probe experiments *Phys. Rev. Lett.* **102** 136401
[48] Kemper A F, Sentef M A, Moritz B, Freericks J K and Devereaux T P 2015 Direct observation of higgs mode oscillations in the pump-probe photoemission spectra of electron-phonon mediated superconductors *Phys. Rev.* B **92** 224517
[49] Nosarzewski B, Moritz B, Freericks J K, Kemper A F and Devereaux T P 2017 Amplitude mode oscillations in pump-probe photoemission spectra from a d-wave superconductor *Phys. Rev.* B **96** 184518
[50] Xu T, Morimoto T, Lanzara A and Moore J E 2019 Efficient prediction of time- and angle-resolved photoemission spectroscopy measurements on a nonequilibrium bcs superconductor *Phys. Rev.* B **99** 035117
[51] Schwarz L, Fauseweh B and Manske D 2020 Momentum-resolved analysis of condensate dynamic and higgs oscillations in quenched superconductors with time-resolved arpes *Phys. Rev.* B **101** 224510